

## **Wave energy dissipation due to mudbanks formed off southwest coast of India**

**Samiksha S. V.<sup>\*a</sup>, P. Vethamony<sup>a</sup>, W. Erick Rogers<sup>b</sup>, P. S. Pednekar<sup>a</sup>, M.T. Babu<sup>a</sup>, P.K. Dinesh Kumar<sup>c</sup>**

<sup>a</sup>Physical Oceanography Division, CSIR-National Institute of Oceanography, Dona Paula, Goa – 403004, India.

<sup>b</sup>Naval Research Laboratory (NRL) Oceanography Division; Code 7322; Stennis Space Center, MS 39529, USA.

<sup>c</sup>CSIR-National Institute of Oceanography, Regional Centre, Kochi, Kerala – 682018, India.

\*Corresponding author: Samiksha S.V.: vsamiksha@nio.org Tel.: +91 832 2450296; Fax: +91 832 2450608.

### **Abstract**

Mudbanks (MBs) are a unique natural phenomenon, and form along the southwest coast of India during the southwest monsoon. They are characterized by a calm-water region, bordered by a rough sea. In order to quantify the wave energy dissipation, wave data were collected at two water depths (15m and 7m) before and during the period of formation of MBs off Alappuzha, Kerala. The observations indicate that MBs exist even in deeper water beyond 15m water depth, contrary to earlier findings that they only form in depths of 0-5m. The analysis showed 65-70% wave height attenuation. As spectral density evolves with shoaling, energy dissipation was examined using the concept of wave energy flux. The combination of high frequency dissipation and nonlinear energy transfer from higher-frequency to low-frequency waves resulted in a reduction of energy across a wide frequency range. The WAVEWATCH III® (WW3) model with wave-mud interaction physics was used to capture the signature of wave energy dissipation due to MBs. The accuracy of prediction of significant wave heights ( $H_s$ ) of the WW3 model was verified using  $H_s$  of measured waves and ERA- Interim (ECMWF Reanalysis Interim data). The model accurately reproduced both the wave heights in the MB region and their general characteristics. The measurements and model results complement each other in explaining changes associated with an apparent shift of the MBs.

**Keywords:** mudbanks; wave energy dissipation; wave modelling; Wavewatch III; wave-mud interaction; wave energy flux

## Introduction

Mudbanks (MBs), defined as a temporary accumulation of dense fine suspended sediments, cause a calm-water region in nearshore waters, devoid of any significant wave action. MBs are a unique phenomenon that occurs at only a few locations in the nearshore waters of the world oceans. MBs off Alappuzha, Kerala are considered a unique formation as they occur in a non-estuarine region. Similar formations are reported off the Yellow River delta in the Bohai Sea of China (Ren and Shi, 1986), near the Amazon River mouth along the northeast coast of Brazil and in Guyana (Allison et al., 2000). These take the form of a permanent muddy-bottom near the river mouth, unlike Alappuzha MB, which is far away from any estuary. Along the coast of India, MBs are known to occur only on the Kerala coast, and locally known as “Chakara”. Along the Kerala coast, MB usually forms approximately at 12 specific regions, including Alappuzha during the southwest monsoon (June-August) when wave heights are very high compared to other seasons (Mathew et al., 1995). It may be noted that Kerala MBs will not form in all 12 locations in the same year. The MB appearing off Alappuzha has socio-economic implications as it has long been known for its very high biological productivity (Damodaran, 1973; Gopinathan and Qasim, 1974; Nair et al., 1984; Rao et al., 1984; Thompson, 1986); also, it prevents the occurrence of rapid coastal erosion (Kurup, 1977; Silas, 1984; Nair, 1976) during the southwest monsoon season.

Previous investigations of MBs cover the salient hydrographic features and some of the physical processes involved in different stages of MB evolution (Kurup, 1977; CMFRI, 1984; Mallik et al., 1988; Ramachandran, 1989). Although a number of studies/hypotheses were conducted/proposed for the origin, formation, maintenance and disappearance of the MB off Kerala, the phenomenon is not yet completely understood (Nair, 1976; Wells and Coleman, 1981; Silas, 1984; Wells and Kemp, 1986; Froidefond et al., 1988; Faas, 1991, 1995; Mehta and Jiang, 1993; Mathew et al., 1995; Mathew and Baba, 1995). Tatavarti and Narayana (2006) conducted experiments in the MB regions during monsoon and non-monsoon seasons to understand their dynamics and indicated that the prevailing local meteorological conditions are also important in their formation. Philip et al. (2013) studied the meteorological aspects associated with the formation of MB, and found that formation is associated with increased upwelling along the coast. Another hypothesis for the formation is subterranean flow of mud from the adjacent lake (Menon, 1924; CMFRI, 1984, Balachandran, 2004). Recently, Jacob et al. (2015) and Loveson et al., (2016) argued over the validity of subterranean conduit flow of mud/water from the Vembanad Lagoon.

Waves of shallow and intermediate depths interact with the seabed at spatial and temporal scales defined by wavelength and period. Waves exert pressure on the seabed, and in the case of a

fluidized mud seafloor, the bed moves, resulting in dampening of incoming waves by the fluid mud layer. A few theoretical and laboratory studies have been carried out on wave energy dissipation by mudbanks off Kerala coast over a cohesive bottom (Reddy and Varadachari, 1973; MacPherson and Kurup, 1981; Sheno and Murty, 1986). Mathew et al. (1992, 1995, 1995) based on wave and current measurements off Alappuzha during fair and SW monsoon weather conditions opined that MB dynamics, i.e. formation, growth, transport and dissipation, is mainly governed by the wave field and weak currents that occur in the formation region. They observed that in the developing and dissipating stages of the mudbanks, wave height attenuation was about 75-85% in the nearshore recording station, and almost 100% just before reaching the shoreline. This dissipation is due to the presence of fluidized mud layer at the bottom, rather than the effect of bottom friction, which normally dissipates wave energy in shallow waters (Mathew, 1992). Faas (1995) argued that the characteristic variations in suspended sediment concentration with seasonal progression of monsoonal waves and bottom conditions correlate with the rheological response of bottom mud to wave forcing. Jiang and Mehta (1995) showed that the rheology of bottom mud from the area can be described by a viscoelastic model, which is a generalization of the Voigt model for mud proposed by Maa (1986). The model of Mehta and Jiang (1993) does not take into consideration the three dimensional nature of the wave field and the changing rheology of the mud in the spatial and temporal environment. Shynu et al. (2017) carried out seasonal time series measurements of suspended particulate matter (SPM) concentrations at various locations in the mudbanks and non-mudbanks areas and found that the mean SPM concentrations were low at surface and mid-depth waters and relatively high at bottom-depth waters at both mud bank and non-mud bank stations during pre-monsoon and monsoon seasons. This study postulated that the dissipated wave energy might have probably eroded the bottom sediment and formed the near-bed fluid mud.

Many theoretical models for wave-mud interaction have been proposed, involving a range of rheologies and dissipation mechanisms. Mud has been described as a viscous Newtonian fluid (Dalrymple and Liu, 1978; Ng, 2000; De Wit, 1995), viscoelastic solid (Jiang and Mehta, 1995), viscoplastic bingham material (Mei and Liu, 1987; Chan and Liu, 2009) and poroelastic material (Yamamoto and Takahashi, 1985). In the past few decades, many researchers have examined the physical processes involved in wave-mud interaction, including wave-induced mud transport (e.g., Vinzon and Mehta, 1998; Traykovski et al., 2000, 2007; Hsu et al., 2009; Jaramillo et al., 2009; Safak et al., 2010; Siadatmousavi et al., 2012) and surface wave attenuation (e.g., Dalrymple and Liu, 1978; Winterwerp et al., 2007; Elgar and Raubenheimer, 2008; Rogers and Holland, 2009; Kranenburg et al., 2011, Sheremet et al., 2011; Hsu et al., 2013, among many others) through

measurements and numerical modelling. Other processes such as nonlinear interaction between surface and interfacial waves at the water-mud separation surface (Jamali et al., 2003), in addition to viscous dissipation in the mud layer, have been hypothesized to contribute to wave damping. Various methods (Gade, 1958; Dalrymple and Liu, 1978; Ng, 2000) exist for estimating the damping of water waves by viscous mud. But, treating non-rigid seafloor as a viscous fluid do have limitations: mud can also exhibit viscoelastic or plastic behaviour (Hsiao and Shemdin, 1980; Jiang and Mehta, 1995 and 1996; Zhang and Ng, 2006; Winterwerp et al., 2007). Though different hypotheses were proposed for explaining the formation of MB, none of them is conclusive. Our present focus is not on the formation of MB, but rather, on wave energy dissipation due to MB through measurements and modelling.

Representation of damping of waves over muddy seabed is introduced in WAVEWATCHIII®(WW3) model, which has two physics: (i) a numerical solution derived by treating the mud as a laminar viscous fluid (Dalrymple and Liu, 1978) (hereinafter referred to as DL) and (ii) an analytical and asymptotic solution, simplified according to DL, which assumes that mud layer is thin (Ng, 2000). Rogers and Holland (2009) used these mud modules in another wave model, SWAN (“Simulating Waves Nearshore”, Booij et al., 1999) for the Casino beach, Brazil. The dissipation of waves by a non-rigid bottom was represented in the wave model by treating the mud layer as a viscous fluid. It was found that the model without this type of dissipation has a strong tendency to over-predict nearshore wave energy, except those of large storm waves. They also used an inversion methodology to infer an alternate mud distribution which, when used with the wave model, yielded the observed wave heights.

Considering the importance of mudbanks, which remain in the nearshore zone for a few months during the SW monsoon when productivity is very high (not only in the MB region, but also further offshore), and considering also that the economy of the coastal region during this rough season largely depends on the arrival of MB (to use it as a platform for the fish harvest), the CSIR-NIO initiated a multi-disciplinary oceanographic program, “Alappuzha Mudbanks Process Studies (AMPS)” in 2014 (still ongoing). Under this program, two wave rider buoys were deployed in the MB region (measurements such as water level, currents and winds were also carried out). Simultaneously, chemical, geological and biological studies/samplings/ measurements were also conducted during this event. The objectives of this study are: (i) deriving the salient features of mudbanks-attenuated waves from the measured data, (ii) studying the shifting/oscillating nature of MB, which was previously speculative and (iii) modelling the complex phenomenon of MB-induced wave energy dissipation by incorporating the mud-wave interaction processes.

## **2. Data and Methodology**

### **2.1 Data**

#### **2.1.1 Measured data**

The Alappuzha coast (Figure 1c) is a prograding coastline with wide sandy beaches to the north and narrow sandy beaches to the south. The hinterland is marshland underlain by fine sediments. The shelf is narrow, and beach ridges exist at 20m water depth. The shelf gradient is gentle, and 10m and 20m isobaths are at about 5 km and 10 km distance from the shore (Narayana et al., 2008).

At times, it is difficult to fix the exact location as well as time of formation of the mudbanks. Previous studies (Mathew et al. 1992, 1995a; Narayana et al., 2008; Elgar and Raubenheimer, 2008) considered that MB forms within 6 km from the coast, which is approximately at 5m depth. Anticipating the formation of MB off Alappuzha coast, one Datawell directional wave rider buoy was deployed at 15m water depth (location B1) on 21 May 2014, and wave data were collected up to 31 July 2014, covering the pre-mudbanks scenario and mudbanks evolution stages (Fig. 1b & d). Another buoy was deployed at 7m depth (location B2) on 26 June 2014 (after the formation of MB), and wave data were collected till 31 July 2014 (Figure 1b). The locations B1 and B2 were at a distance of 10km and 6km from the shore, respectively. Wave data were collected for 10 minutes duration at 30 minutes intervals. The wave rider buoy has an accuracy of 3% for wave height and within  $0.5^{\circ}$ – $2^{\circ}$  for wave direction.

Simultaneous wind measurements were carried out by installing an Autonomous Weather Station (AWS) of CSIR-NIO on the coast, very close to the wave rider buoy mooring. The AWS (Autonomous Weather Station) provided wind speed and direction at 10 minutes intervals. The accuracy of AWS is: 0.2 m/s for wind speed in the range 0-60 m/s and  $3^{\circ}$  for wind direction.

#### **2.1.2 Mud rheological parameters**

Mathew (1992) measured rheological parameters of the Alappuzha MB, and studied various factors related to wave attenuation and suspended sediments. These measured parameters were used by Jiang and Mehta (1996) in their model to predict wave attenuation. The rheological parameters for the present study were fixed based on the above data and the present field survey. Mud density in the mudbanks region generally ranged between 1,080 and 1,300 kg/m<sup>3</sup> (Mathew 1992; Fass 1995; Jiang and Mehta 1996). It was reported that the dynamic viscosity of upper fluid mud obtained in the initial stage of MB formation was 4.76 Pa-sec, about 4,000 times greater than the viscosity of seawater. Based on the above, the kinematic viscosity of the mud layer was estimated for the present study:

values ranging from 0.0031 to 0.0043 m<sup>2</sup>/s were also tested. Though mud layer thickness was not measured during the present field work, it was confirmed with the field team that it was around 0.4-0.5m at B1. The size of mud patch was set at 35 km x 13 km in the modelling (Figure 1d) to represent the estimated geographical extent of the MB. We have finalized the size of mud patch based on field observations and years of experience of the local people; we suppose that the size is very close to the real scenario.

## 2.2 Model

### 2.2.1 WW3 model description

WW3 model (version 4.18) is a fully spectral third generation model, used at global and regional scales (Tolman 1991; Tolman et al. 2014). The governing equation of the model is the wave action density spectral balance equation, which can be written in a spherical grid as,

$$\frac{\partial N}{\partial t} + \frac{1}{\cos \phi} \frac{\partial}{\partial \theta} \dot{\phi} N \cos \theta + \frac{\partial}{\partial \lambda} \dot{\lambda} N + \frac{\partial}{\partial k} \dot{k} N + \frac{\partial}{\partial \theta} \dot{\theta}_g N = \frac{S}{\sigma} \quad (1)$$

$$\dot{\phi} = \frac{c_g \cos \theta + U_\phi}{R}$$

$$\dot{\lambda} = \frac{c_g \sin \theta + U_\lambda}{R \cos \phi}$$

$$\dot{\theta}_g = \dot{\theta} - \frac{c_g \tan \phi \cos \theta}{R}$$

where,  $N(k; x, t)$  is the wave number spectrum,  $k$  is wave number and  $\theta$  is wave direction;  $\lambda$  and  $\phi$  are the longitude and latitude;  $\sigma$  is the intrinsic wave frequency;  $c_g$  is the group velocity;  $R$  is the radius of earth;  $U_\lambda$  and  $U_\phi$  are the longitude and latitude components of mean current speeds.

The net source term  $S$  generally consists of four parts: a wind-wave interaction term  $S_{in}$ , a nonlinear wave-wave interaction term  $S_{nl}$ , a breaking dissipation term  $S_{ds}$  and a wave-bottom interaction term  $S_{bot}$ . In shallow water, depth-induced breaking ( $S_{db}$ ) and triad wave-wave interaction ( $S_{tr}$ ) become important. This defines the general source terms used in WW3 as,

$$S = S_{in} + S_{nl} + S_{ds} + S_{bot} + S_{db} + S_{tr} \quad (2)$$

The WW3 wave model, which is relatively efficient for larger scales (e.g. global), was selected for the study as our earlier studies (Aboobacker et al., 2011; Samiksha et al., 2012) showed that incorporating swells propagating from the Southern Ocean to the northern Indian Ocean increased the model accuracy. For our smaller domain (inner nest), we decided to also use a WW3

implementation, since the SWAN manual (User manual, Cycle III, 41.01A) states that nesting of SWAN with WW3 is still not a fully tested process.

### 2.2.2 Dissipation by viscous mud: mud module in WW3

Two formulations for wave damping by viscous fluid mud have been implemented in WW3 (Rogers and Orzech, 2013; Tolman et al., 2014) based on earlier implementations in SWAN by Rogers and Holland (2009). The first formulation is by Dalrymple and Liu (1978), hereafter referred to as DL. It is a numerical solution, which treats the mud as a laminar viscous fluid. This is relatively an accurate method, but requires a complex iterative technique, which significantly lengthens computational time. Wave dissipation by fluid mud is computed using an iterative procedure that converges to the complex mud-induced wave number,  $k_{mud}$ . Dissipation due to mud at each frequency is determined from the imaginary part of this wave number as,

$$D_{mud} = 2 \cdot \text{imag}(k_{mud}) \cdot C_{g,mud} \quad (3)$$

where,  $C_{g,mud}$  is the mud-induced wave group velocity. This dissipation is added to contributions from other source/sink terms. For additional details on the derivation of this source terms, readers may refer to Dalrymple and Liu (1978).

The second formulation is by Ng (2000), hereafter referred to as Ng. It is an analytical, asymptotic solution, simplified according to DL, and assumes that the mud layer is thin with respect to the upper water layer. This formulation computes a mud-induced group velocity from the real part of the mud-induced wave number, and allows the effects of mud on wave refraction and shoaling. The Ng method determines two second-order coefficients ( $B'_r, B'_l$ ) that are then used to compute wave attenuation due to mud as,

$$D_{mud} = \text{imag}(k_2) = -\frac{\delta_m (B'_r + B'_l) k_1^2}{\sinh 2k_1 h + 2k_1 h} \quad (4)$$

where,  $\delta_m$  is the Stokes boundary layer thickness for mud,  $h$  is water depth and  $k_1$  and  $k_2$  are the first- and second-order parts of the wave number, respectively in a Taylor expansion about the mud-water interface. For additional details, readers may refer to Ng (2000).

Both these methods are operated by solving for a modified dispersion relation, where the wave number is being solved for complex mud-induced wave number. A key feature of the implementation in WW3 (Rogers and Orzech 2013) is that the mud variables, namely, mud thickness, density and kinematic viscosity are allowed to be non-stationary and non-uniform in space

and time. Both modules neglect elasticity in the mud layer. Mud thickness should be interpreted not as the total mud thickness, but rather as the thickness of the fluidized mud layer.

### 2.3 Model domain and set-up

Two model domains were used: the outer domain (Figure 1a) covers the entire Indian Ocean from 60°S to 30°N and 15°E to 130°E with a spatial resolution of 0.5°×0.5°(≈55×55 km). This domain accommodates the swells coming from the south Indian Ocean, including the Southern Ocean, approaching the shallow region off Alappuzha. The input winds were taken from ERA-Interim database with the same resolution. The inner model domain (Figure 1b) covered the region from 75°E to 77°E and 8°N to 11°N with a spatial resolution of 0.03°×0.03°(≈3×3 km). ERA-Interim winds, of resolution 0.125°×0.125° (≈14×14 km), were given as input to the inner domain. Bathymetry was generated using the ETOPO1 Earth Topography (1 minute) data obtained from the National Geophysical Data Centre, USA for the outer domain and the inner domain bathymetry was further improved by augmenting the digitized NHO (Naval Hydrographic Office, Dehra Dun, India) bathymetry charts (NHO Chart no. 222). The wave rider buoy locations B1 and B2 were separated by a distance of ≈4 km. The model grid resolution is 0.03°×0.03° (≈3km) for the inner domain. Because of this, the extracted model output at B2 is same as that at B1. Hence, model  $H_s$  comparison is shown only for B1 in all figures. Further,  $H_s$  of ERA is extracted at 0.125°×0.125° (≈14km) grid resolution, and therefore, both the locations B1 and B2 exist in the same grid. If finite mesh would have been used, probably we would have got better results than the present rectangular grid model output.

The model was discretized into 40 frequency bins ranging from 0.025 to 1.1 Hz on a logarithmic scale and 24 direction bins having an angular resolution of 15°. The standard third-generation physics were applied with higher order propagation schemes from Tolman (2002). In order to accommodate bias in forcing wind fields, the improved parameterization of Ardhuin et al. (2010) with wind input parameter  $\beta_{\max} = 1.45$  was used, and several test cases were carried out by adjusting the  $\beta_{\max}$  parameter, and we found that  $\beta_{\max} = 1.45$  underestimated the wave heights at the measurement location B1; however, when it was tuned to  $\beta_{\max} = 1.55$ , yielded better results. The quadruplet non-linear wave-wave interaction is computed using the Discrete Interaction Approximation theory (Hasselmann et al., 1985). The model was initiated with depth-induced breaking physics by Battjes and Janssen (1978). This inclusion of algorithms is intended to extend the applicability of the model to shallow water environments, where surf breaking, among other depth-induced transformation processes, becomes important. The bottom friction in WW3 is



calculated based on modified values of SHOWEX formulation by Ardhuin et al. (2003). This formulation is used in our study for no-mud condition only, for comparing with simulations using DL and Ng formulations. The directional wave spectra boundary conditions for the inner domain were generated from the outer domain.

The interaction of waves with mud in the MB region has been studied using the two modules introduced in the WW3 model and the field measurements. Initially, no-mud condition has been considered. For this, WW3 model significant wave heights ( $H_s$ ) of no-mudbanks formation condition were validated with  $H_s$  of measured data collected before the formation of mudbanks and also with  $H_s$  extracted from the ERA-Interim database (Dee et al. 2011) as ERA-I derived  $H_s$  does not account for the MB condition.

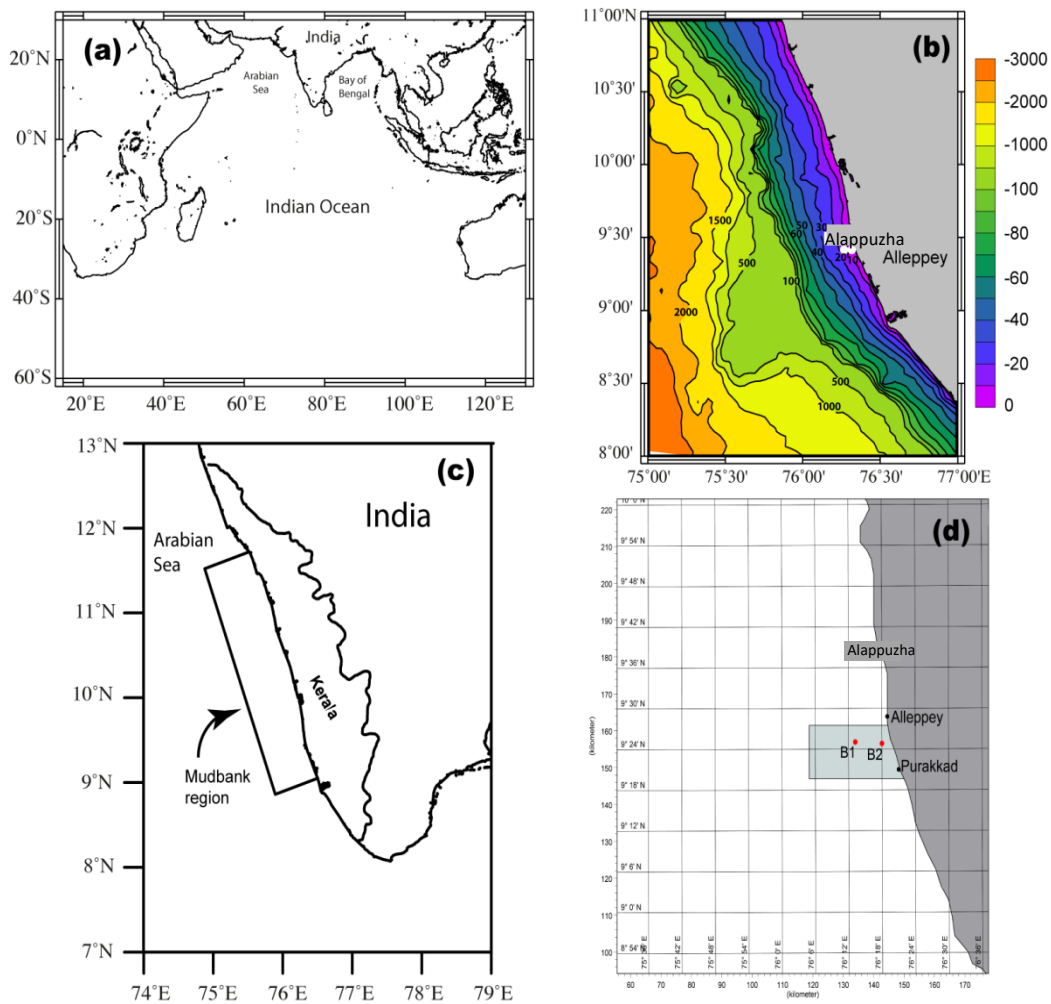


**Figure 1.** (a) The outer domain covering the Indian Ocean; (b) Inner domain with bathymetry details and wave rider buoy moored locations, B1 and B2; (c) The box covers all the 12 mudbanks regions (not to scale) off Kerala; (d) Mud patch introduced in the model.

### 3. Results and discussions

#### 3.1. Characteristics of waves in the mudbanks region from measurements

The daily measured significant wave height, mean wave period and peak wave direction at two water depths, 15m (B1) and 7m (B2), are presented in Figure 4. As the wave rider buoy at 7 m was deployed after the formation of MB, no data was available prior to 26 June 2014 at this location. At the location B1, the maximum significant wave height ( $H_s$ ) observed was 3.16m and minimum 0.76m with peak wave periods ranging from 6 to 20s (mean wave periods varied between 4 and 10s) and predominant wave direction between  $200^\circ$  and  $280^\circ$  (propagating towards NNE and ESE directions). Similarly, at location B2, the maximum and minimum  $H_s$  were 1.56m and 0.68m, respectively, with peak and mean periods similar to B1, and predominant wave direction between  $200^\circ$  and  $250^\circ$  (NNE and ENE). Wind speed and direction were plotted to note the variation during the period of MB formation; mean and maximum wind speeds were 1.5m/s and 12.2m/s, respectively; dominant wind direction was  $300^\circ$ .

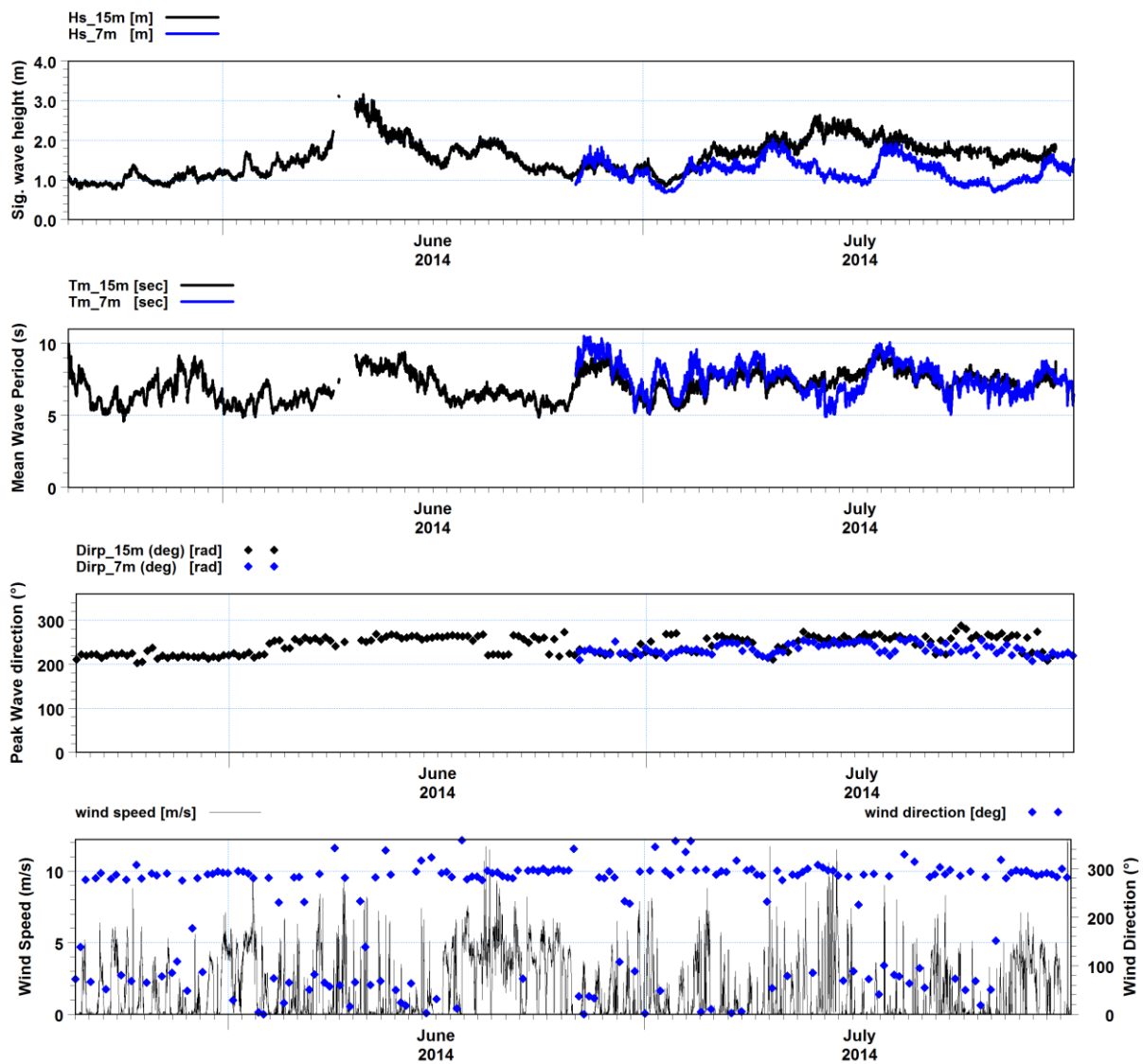


**Figure 2.** Wave parameters measured at 15m (B1) and 7m (B2) water depths; also shown is wind speed and direction (bottom panel) measured using an AWS at a nearby coastal station.

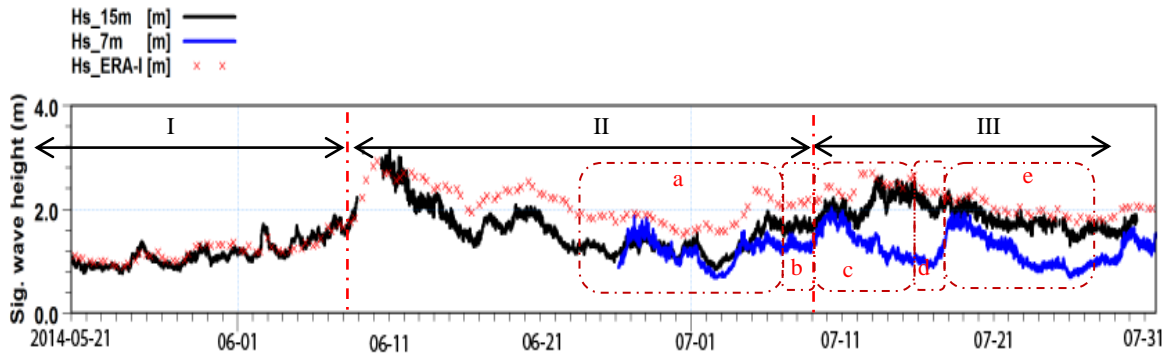
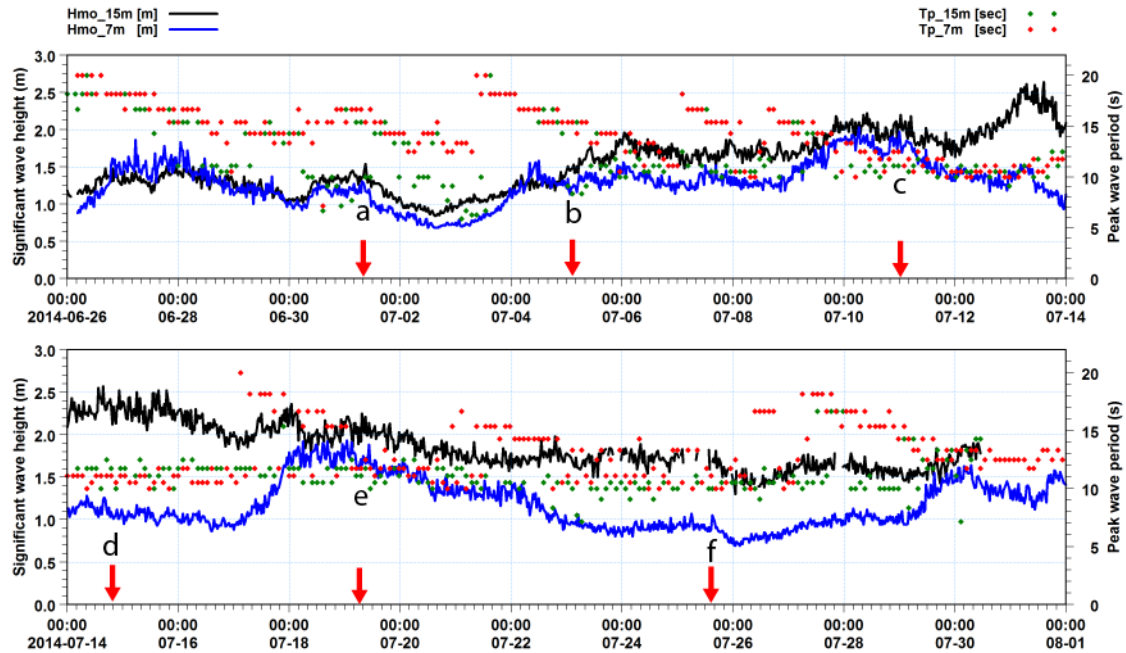


**Figure 3.** Measured  $H_s$  plot is divided into time segments as I, IIa, IIb, IIIc, IIId and IIIe in order to explain the dynamics of MB at the measurement locations and subsequent wave energy dissipation.

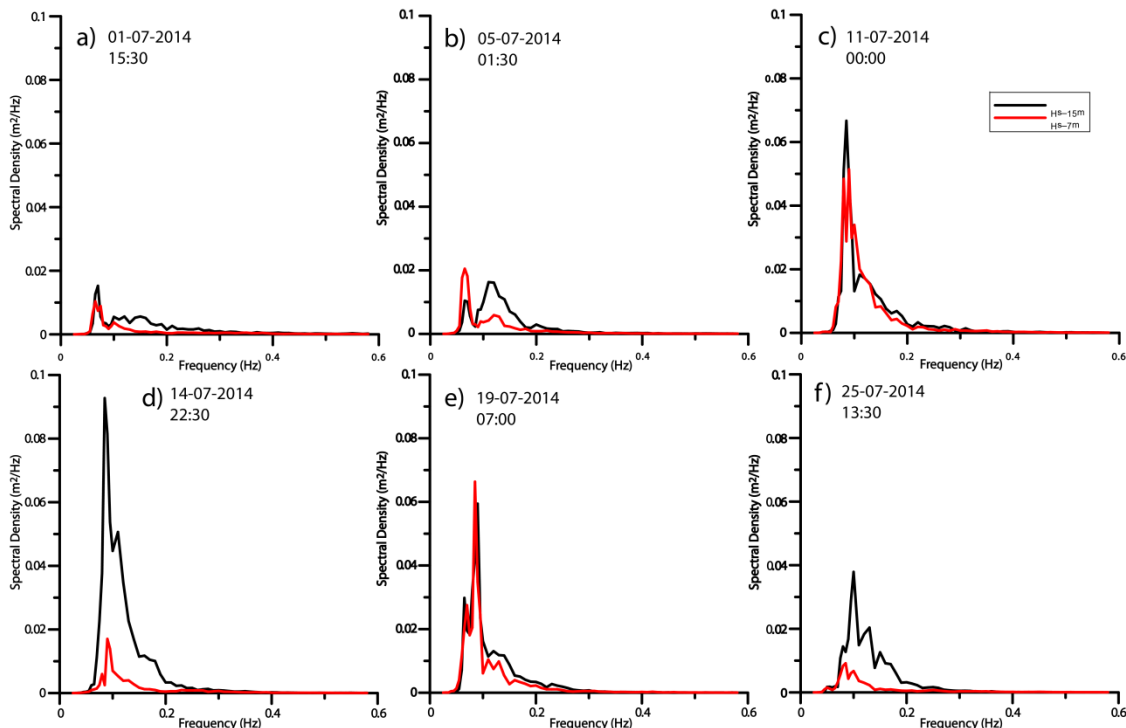
The measured  $H_s$  with time were divided into different time segments, I, IIa, IIb, IIIc, IIId and IIIe as shown in Figure 3 in order to explain the dynamics of MB at the measurement locations and subsequent wave energy dissipation. It was observed that during 21 May to 11 June (Part I), the measured  $H_s$  at B1 matches well with the ERA-Interim  $H_s$ , proving the accuracy of both measurements and ERA-I model results, as well as indicating that MB was not yet formed at B1. Interestingly, measured  $H_s$  between 12 June and 11 July 2014 (Part II) were found to be less than the ERA-Interim  $H_s$ , suggesting the arrival of MB at B1. The buoy at B2 was not deployed at this time, so it was not known when MB formed/arrived at B2. After 11 July (at the end of Part II), again  $H_s$  of ERA-Interim match well with B1 data, suggesting a shift of the MB from B1. It is noticed in Figure 3 that wave heights at 7m depth are lesser than those at 15m for most part of the time, with reduction of wave heights at B1 and B2 remaining nearly the same during 25 June - 11 July 2014 (a&b) relative to ERA- Interim wave heights, which represent no-mud condition. It is also observed that there was significant reduction in wave heights at B2 during IIIc and IIIe, and wave heights at B1 virtually returned to no-MB condition.  $H_s$  increased at B2 for small duration during IIb and IIId, which may indicate shifting of the MB from B2. The wave period is not consistently different in IIb and IIId relative to IIIc and IIIe, and therefore, change in apparent impact of the mud is not easily attributed to change in incident wave period. It may be noted that due to restriction in the model resolution, this shifting nature of MB is explained only with the measured data.

Mathew et al. (1995) reported that in developing and dissipating stages of the MB, wave heights were attenuated about 75-85% by the time the waves reached the near-shore recording station (5m water depth) and almost 100%, before they reached the shoreline. In the present study, a maximum reduction of 65-70% at B2 (depth = 7m) was observed, implying that MB activity has reduced relative to earlier years. Visual observations during the field visits and personal discussions with fishermen also gave the impression that water was less muddy and turbid in the 2014 MB region, compared to earlier years; also, monsoon was weak in 2014 in the Kerala State. It was

speculated that MB form within 5-6 km (water depth = 5m) from the coast. The present study confirmed that MB can form even beyond 10km from the coast (water depth >15m).



**Figure 4.** Variation of  $H_s$  and  $T_p$  measured at 15m (B1) and 7m (B2) water depths during wave energy dissipation in the MB region. This part of the figure is expanded from Part II (a&b) and Part III (c,d&e) of Figure 3 to illustrate the wave spectral behaviour at B1 and B2.



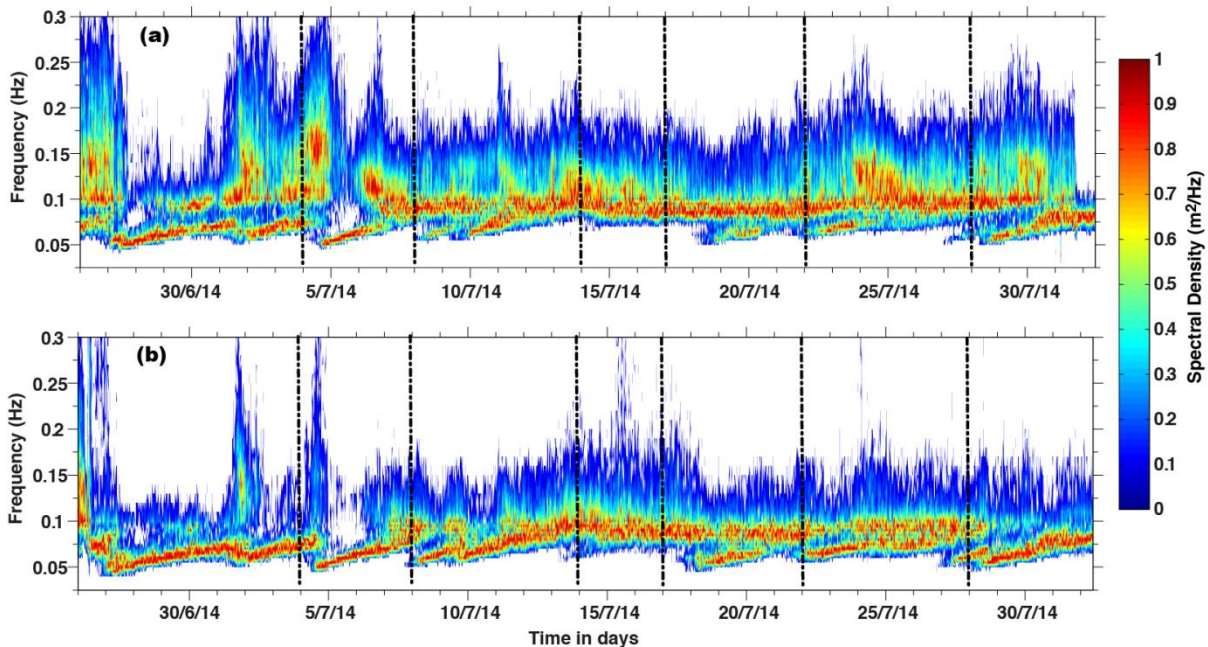
**Figure 5.** Typical measured wave spectra during the MB period: (a) 01-07-2014, (b) 05-07-2014, (c) 11-07-2014, (d) 14-07-2014, (e) 19-07-2014 and (f) 25-07-2014 at B1 and B2.

Figure 4 presents the observed wave height and period at the two locations in greater detail, showing only the time periods corresponding to IIa through IIIe. To further analyse the evolution of wave energy dissipation as well as wave spectral behaviour before, during and after the MB formation between the two buoy locations B1 and B2, we selected a few typical wave energy spectra at both the locations, corresponding to the times marked as a, b, c, d, e and f in Figure 5. During this time, at both locations, peak wave period ranged from 10s to 18s (with a few outliers), indicating the dominance of long period waves. In general, peak periods are shorter at 15m water depth compared to 7m depth. All the wave spectra presented in Figure 5 show that there was considerable dissipation in the wind sea part of the spectrum when waves travelled from 15m to 7m depth. The wave spectrum presented in Figure 5b shows that wind sea part of the energy was higher at 15m depth compared to 7m depth, and this is because wind was blowing towards shore, that is, approximately  $300^\circ$  (wind direction is presented in the lower panel of Figure 2). Low frequency energy was higher at 7m compared to 15m (Figure 5b). This might have been caused by nonlinear energy transfer or shoaling. At the same time, it is very clear that (Figure 5 (d, f)), when the MB was very active in a region, there was a reduction in energy across all frequencies. In this discussion, it is useful to keep in mind the relative water depth ( $kh$ ) of the wave frequencies shown. The transition from deep to shallow water may be taken as  $kh = 3.14$  to  $0.25$ . If we take central value of  $kh=1.5$  as a semi-arbitrary point of reference, separating “more bottom effects” from “less bottom effects”, that corresponds to frequencies of 0.22 Hz and 0.15 Hz for depths of 7m and 15 m, respectively. This indicates that waves at B2 (7m) are significantly affected by the seafloor across the entire energy-containing range of spectra shown in Figure 5; for waves at B1 (15 m), the affected frequencies include all of the primary swell peak and a large portion of the secondary wind sea peak.

As waves propagate into shallow water, the nonlinear interactions approach resonance, allowing large and rapid transfer of energy from higher to lower-frequency motions (Sheremet et al. 2005; Kaihatu et al. 2007; Elgar and Raubenheimer 2008), where dissipation rates will be much greater. According to the above studies, the combination of high frequency dissipation and nonlinear energy transfer from higher-frequency waves to low frequency waves can result in reduction of energy across a wide frequency range, including waves that are too short to “feel the bottom”. Our observations are in agreement with the earlier studies as dissipation is readily apparent in the higher frequencies. However, as “higher frequencies” in previous studies were in deep water, and ours were not, it is impossible to conclude whether the observed decrease of energy at high frequencies (e.g. Figure 5b) is caused by linkage with longer waves, which were strongly affected by the seafloor or by direct interaction with the seafloor.

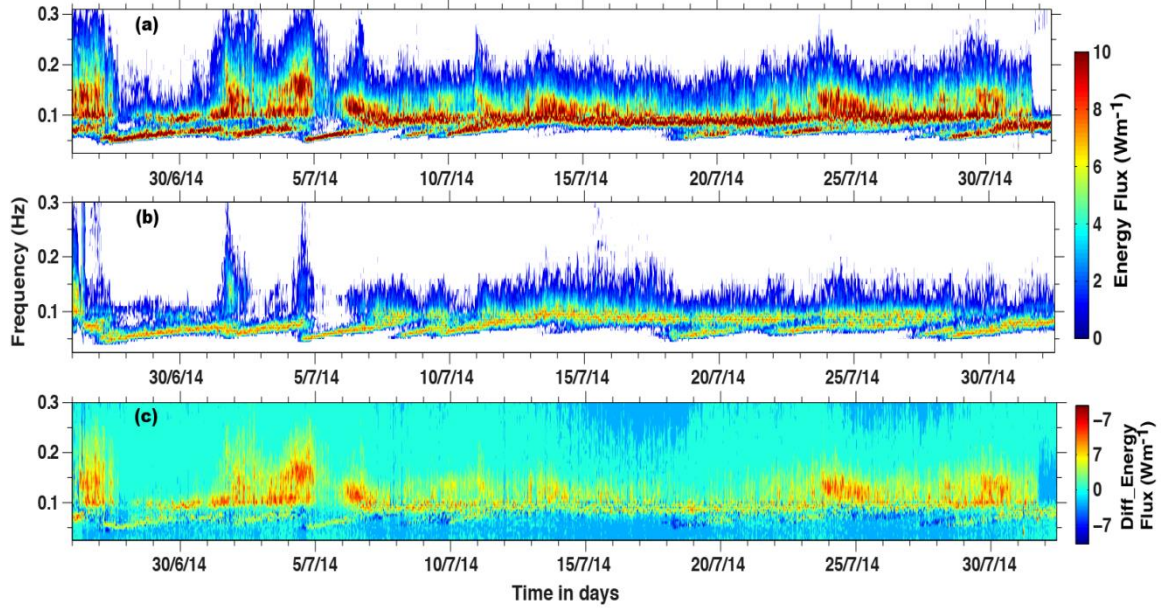
Figure 5 (c, e) is illustrative of the situation in which there is little change in energy level from waves propagating from B1 to B2, implying little or no dissipation by mud, suggesting that the MB is offshore of B1 during this period. The spectral distribution is similar at the two locations (Figure 5c, e), suggesting that nonlinear interactions are not redistributing much energy within frequencies between B1 and B2 locations.

Figure 6 is the normalised wave spectra showing the evolution of spectral energy at the two water depths during MB formation (26 June to 31 July 2014). Being a normalized plot, it does not distinguish between, for example, zero dissipation vs. equal dissipation at all frequencies. One feature is very noticeable: on days 1 July, 5 July and 25 July 2014, reduction in energy has occurred in the higher frequency peak. This is consistent with the behaviour seen in the non-directional spectral plots (Figure 5 a, b).



**Figure 6.** Evolution of wave frequency spectrum during mudbanks formation at the two water depths off Alappuzha: (a) 15 m (location B1) and (b) 7m (location B2).

So far, we have mentioned two possible roles of nonlinear interactions in these observations, both involving transfer of energy from high to low frequency; first is the increase in energy at low frequency in Figure 5b, which may also be explained by shoaling; second is the dissipation of shorter waves by mud. The latter can also happen by direct interaction with the seafloor, but the direct interaction may be substantially slower if the short wave is not in relatively shallow water. Also, as noted above, the behaviour in Figure 5 (c, e) seems to argue against a major role of nonlinear interaction. Though the role of nonlinear interaction is unclear here with seemingly contradicting evidence, it is pointed out that these fast near-resonant nonlinear transfers are not represented in the model simulations.



**Figure 7.** Energy fluxes (represented in colour; units  $\text{Wm}^{-1}$ ) based on observations at (a) 15 m depth, (b) 7 m depth and (c) difference between the fluxes at 15m and 7m.

Changes to spectral density are not exclusively caused by dissipation of waves by mud alone; these changes are produced by shoaling process also. For this reason, visual comparison of spectra at the two locations (15 m and 7 m depths), as in Figures 4 and 5, is not the best way to evaluate wave damping by mud. Therefore, in order to evaluate the wave damping between the two locations, we calculated wave energy flux, which is spectral density multiplied by group velocity as a function of frequency,  $E(f)C_g(f)$ . The calculated fluxes at two depths and their differences are shown in Figure 7. This indicates qualitatively that the damping is significant. It is cautioned that this is a scalar representation of energy flux that does not account for the effect wave refraction. A rigorous treatment of energy flux would be in vector form and would include refraction. Third generation wave models, of course, treat all of these effects together, which highlights their utility for quantitative interpretation of observational data.

## 3.2 Wave modelling

### 3.2.1 No mud condition

The WW3 model was set up for no mud condition, and run with the settings described in section 2.3. The WW3 model significant wave heights ( $H_s$ ) were compared with  $H_s$  extracted from the ERA-Interim database (Table 1) at a location of 15m water depth (point B1), and the model results were found to be matching with the observed data (correlation coefficient = 0.97; rmse = 0.19m; bias = -0.14m).

**Table 1.** Statistical comparison of WW3 model  $H_s$  for no-mud condition with ERA-Interim and measured  $H_s$  at 15m water depth (B1).

<b>Comparison</b>	<b>Bias (m)</b>	<b>RMSE (m)</b>	<b>SI</b>	<b>Corr. Coefft.</b>	<b>No. of data points</b>
<b>ERA-Interim vs. WW 3 model</b>	-0.14	0.19	0.1	0.97	282
<b>Measured vs. ERA-Interim</b>	0.32	0.41	0.26	0.86	274
<b>Measured vs. WW 3 model</b>	0.19	0.35	0.23	0.85	274

It is found in Figure 8a that until 11 June 2014, all the three  $H_s$  (measured, ERA-I and WW3 no-mud condition) matched well, proving that WW3 has accurately reproduced the waves for the no-mud condition. An exception is that  $H_s$  of WW3 were underestimated when waves were relatively low ( $H_s < 1.2\text{m}$ ). When waves were relatively high,  $H_s$  of WW3 matched very well with the measurements. As expected, 12 June 2014 onwards, we find over-estimation of  $H_s$  in the ERA-I and WW3 “ $H_s$  no-mud” compared to measured  $H_s$ ; also, a steep reduction is observed in the measured  $H_s$  at B1. These indicate the arrival of MB at B1. Therefore, neither ERA-I nor WW3 “no-mud” (Figure 8a) model could reproduce this MB wave phenomenon; on the other hand, they overestimated  $H_s$  as mud condition was not imposed. This overestimation of  $H_s$  in both ERA and WW3 (rmse = 0.41m; bias = 0.32m for ERA and rmse = 0.35m; bias = 0.19m for WW3) compared to measurements at B1 (Figure 8b) suggests that some type of bottom induced dissipation is needed for accurate reproduction of MB attenuated waves (explained in the next section). Measured mean wave period,  $T_m$  and  $T_m$  of WW3 for no-mud and mud conditions are shown in Figure 8c. There is a good match between the  $H_s$  of model and measurements as shown in Fig. 8 (a&b) both before and after the formation of MB. As found in  $H_s$ , model wave period with mud condition showed good agreement with the measurements than without mud after the formation of MB. Of course, there is a good agreement between model (no mud condition) and measurements, before the formation of MB. The measured peak wave direction,  $D_p$  and mean wave direction,  $D_m$  of WW3 for no-mud and mud conditions are shown in Figure 2d. It may be noted that the peak wave direction of the wave rider buoy is plotted against the mean wave direction of the model, and therefore, it is not surprising that these directions do not match (Figure 8d).



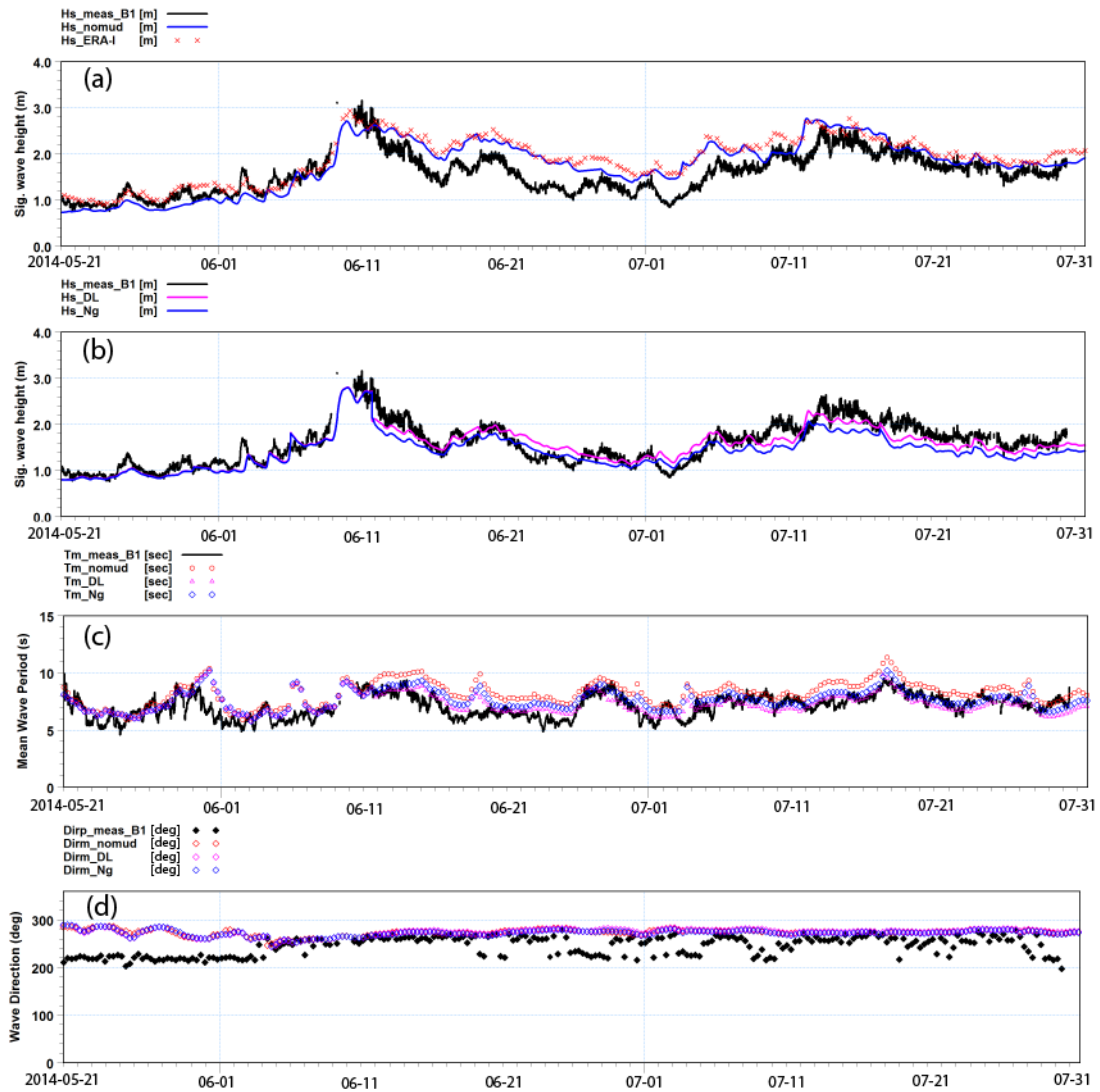


**Figure 8.** Comparison of (a) measured  $H_s$  at B1 (depth=15m) with  $H_s$  of ERA-I and  $H_s$  of WW3 (no-mud condition), (b) measured  $H_s$  at B1 with  $H_s$  of WW3 model (mud condition: DL and Ng), (c) measured  $T_m$  at B1 with  $T_m$  of WW3 (no-mud condition and mud condition) and (d) measured  $D_p$  with  $D_m$  of WW3 (no-mud condition and mud condition).

### 3.2.2 WW3 results using DL and Ng mud modules

A number of numerical experiments were carried out with estimated rheological parameters of mud layer thickness, viscosity and density (Table 2). Model results obtained with the above combinations are presented in Table 2. The scatter plots presented in Figure 9 represent the test cases carried out to select the mud parameters for both the modules.

Figure 9 shows that when the model was setup with the DL module for a mud layer of thickness 0.4-0.5m, viscosity 0.0038-0.0043  $m^2/s$  and mud density 1230-1100  $kg/m^3$ , the model reproduced the wave heights reasonably well (Table 2) (Figure 9 a, b). When a few more experiments were conducted with mud parameters beyond this range, the results were found to be unrealistic. For example, when mud thickness was increased from 0.4m or 0.5m to 0.6m, 0.8m and

1.0m, keeping viscosity and density constant, the model generated waves of the order of 4.5m (Figure 9c). This behaviour indicates sensitivity of the model with DL module to mud layer thickness.

A similar exercise has been carried out with the Ng module in the WW3 model. Initially, mud thickness was varied, and then, both viscosity and density values were varied. The model results showed very small change, when mud thickness was varied in consistent with values considered in the DL experiments (Table 2) (Figure 9 d, e). Further, viscosity and density values were varied to study the behaviour of the Ng module. We find that the best results were obtained for the same combination of mud parameters used in the DL module (Table 2 and Figure 8b). The error level of both the methods was found to be almost the same, except that DL method showed very sharp changes in  $H_s$  when the mud layer thickness was, say, above 0.5 m. The Ng method did not show any change in its performance when the mud layer thickness was varied from 0.4 to 0.5 m. However, performance improved (Table 2: less bias and less rmse) when mud density was increased from 1100 to 1230  $\text{kg/m}^3$ , indicating that Ng is sensitive to density within the parameter range tested. As far as computational time is concerned, the simulation with Ng is 20 to 30 times faster than the DL method.

Table 2. Statistical comparison of measured  $H_s$  with model  $H_s$  for varying mud thickness, viscosity and density for DL and Ng methods (21 May - 31 July 2014).

S. No.	Thickness (m)	Density ( $\text{kg/m}^3$ )	Viscosity ( $\text{m}^2/\text{s}$ )	Bias (m)	RMSE (m)	SI	Corr. Coefft.	n
<b>Dalrymple and Liu</b>								
1	0.4	1100	0.0043	-0.13	0.25	0.16	0.88	3265
2	0.4	1230	0.0038	-0.10	0.23	0.14	0.89	3265
3	0.5	1100	0.0043	-0.11	0.24	0.15	0.88	3265
4	0.5	1230	0.0038	0.08	0.26	0.16	0.84	3265
5	0.6	1230	0.0038	0.36	0.53	0.34	0.74	3265
6	0.8	1230	0.0038	1.29	1.6	1.02	0.56	3265
7	1.0	1230	0.0038	1.66	2.04	1.3	0.54	3265
<b>Ng</b>								
1	0.4	1100	0.0043	-0.29	0.38	0.24	0.85	3265
2	0.4	1230	0.0038	-0.25	0.33	0.21	0.88	3265
3	0.5	1100	0.0043	-0.29	0.38	0.24	0.85	3265
4	0.5	1230	0.0038	-0.25	0.34	0.21	0.87	3265

\*SI=scatter index; n=number of data points

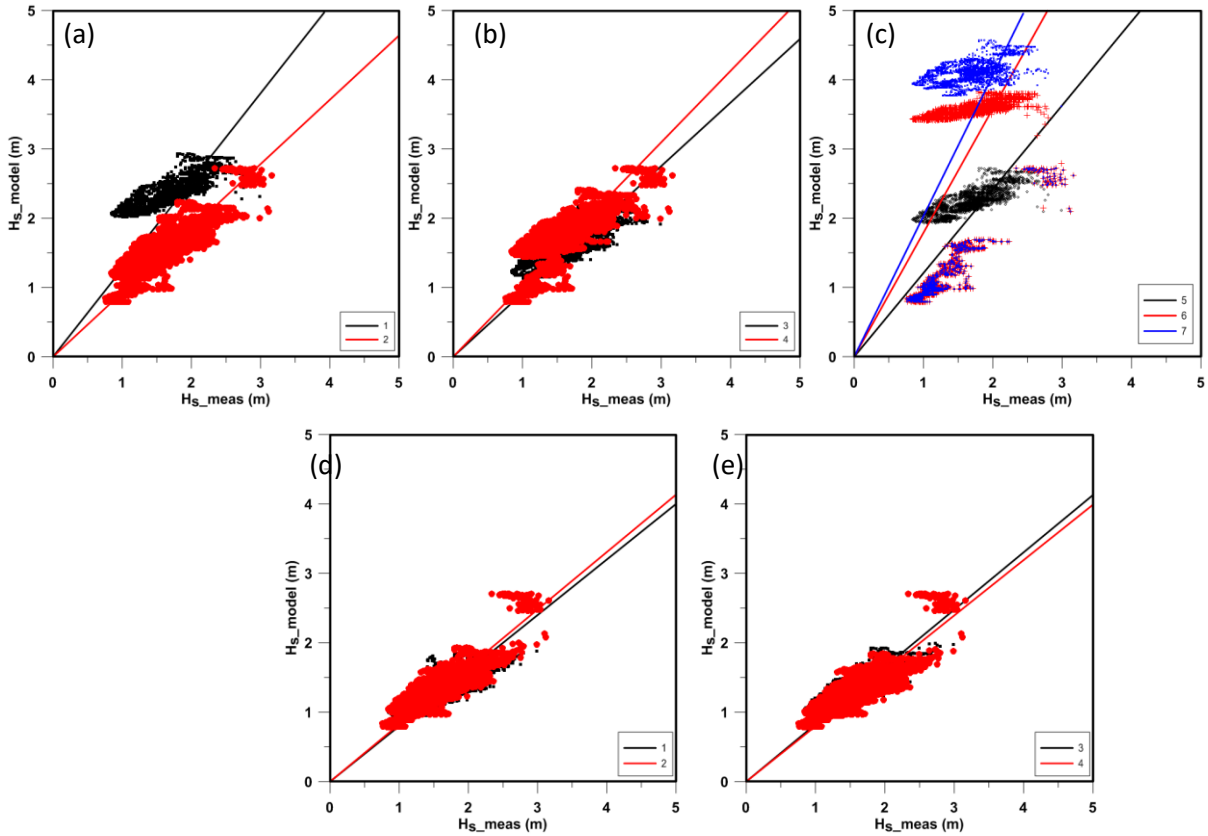


**Figure 9.** Comparison of measured  $H_s$  with modelled  $H_s$  for varying mud viscosity, thickness and density for DL (a, b & c) and Ng (d & e) methods at location B1. Legend numbers correspond to the test cases shown in Table 2.

#### 4. Conclusions

Detailed data obtained from 2014 in the vicinity of a mudbank show that a wave height reduction of about 70% occurred, primarily in the wind-sea part of the spectrum. It was previously speculated that MBs form within 5-6 km (water depth = 5m) from the coast. However, the present study suggests that MBs can form as far as 10km from the coast (water depth >15m), and even further. Our observations are consistent with a scenario in which the combination of high frequency dissipation and nonlinear energy transfer from high frequency to low frequency waves resulted in reduction of energy across a wide frequency range, including waves that are too short to “feel the bottom”. In this sense, our observations are in agreement with earlier studies. The WAVEWATCH III (WW3) model with wave-mud interaction physics captured the signature of wave energy dissipation due to the complex phenomenon of mudbanks off Alappuzha. In the present study, we could not carry out measurements for all the mud properties; however, use of measured data in the modelling removed some of the uncertainties. These results show that field data, combined with careful use of a numerical model of wave-mud interaction, can be used to understand the processes

of formation of mudbanks under a range of conditions, allowing managers and other stakeholders to gain a better understanding of these important coastal features.

## Acknowledgements

We thank Director, CSIR-NIO, Goa for providing facilities to carry out this work. Our special thanks to Dr. S.W.A. Naqvi, former Director, CSIR-NIO for his support and keen interest in this study. The first author acknowledges the DST, India for supporting her research work through WOS-A (SR/WOS-A/ES-17/2012). We acknowledge CSIR-NIO for providing high performance computing domain, HPC-Pravah for running the model. The ERA-Interim wind and wave data were freely downloaded from ECMWF (<http://apps.ecmwf.int/datasets/>). The source code for the model used in this study, WAVEWATCH III, is available on request at (<http://polar.ncep.noaa.gov/waves/wavewatch/>). We thank Mark Orzech (Naval Research Laboratory) for adding the mud routines to the WAVEWATCH III model. We are also thankful to Sudheesh, Lakshmikant and Ravish for their help during field work and Chaitanya and Soumya for assisting in the preparation of figures. We sincerely thank Dr. Steve Mitchell, Editor and the three reviewers for their critical comments which helped us to improve this manuscript to a great extent. The NIO contribution number is xxxx.

## References

1. Aboobacker VM, Rashmi R, Vethamony P, Menon HB (2011) On the dominance of preexisting swells over wind seas along the west coast of India. *Cont. Shelf Res.* 31:1701-1712. doi:10.1016/j.csr.2011.07.010.
2. Allison MA, Lee MT, Ogston AS, Aller RC (2000) Origin of Amazon mudbanks along northeastern coast of South America. *Marine Geology*, 163 (1-4), pp 241–256.
3. Ardhuin F, O'Reilly WC, Herbers THC, Jessen PF (2003) Swell transformation across the continental shelf. Part I: Attenuation and directional broadening. *J. Phys. Oceanogr.* 33:1921–1939
4. Ardhuin F, Rogers E, Babanin A, Filipot JF, Magne R, Roland A, Westhuysen AVD, Queffelec P, Lefevre JM, Aouf L, Collard F (2010) Semi-empirical dissipation source functions for ocean waves: Part I, definitions, calibration and validations. *J. Phys. Oceanogr.* 40:1917-1941
5. Balachandran, KK (2004), Does subterranean flow initiate mud banks off the southwest coast of India?. References and further reading may be available for this article, *Estuarine, Coastal and Shelf Science* 59, 589–598.
6. Battjes JA, Janssen JPFM (1978) Energy loss and set-up due to breaking of random waves. *Proc. 16th Int. Conf. Coastal Eng.* 569–587. ASCE
7. Booij N, Ris RC, Holthuijsen LH (1999) A third generation wave model for coastal regions: I. Model description and validation. *J. Geophys. Res.* 104:7649–7666
8. Chan IC, Liu PLF (2009) Responses of Bingham-plastic muddy seabed to a surface solitary wave. *J. Fluid Mech.* 618:155–180

9. CMFRI (Central Marine Fisheries Research Institute) (1984) Mudbanks of Kerala coast. Bulletin No.31 74p
10. Dalrymple RA, Liu PLF (1978) Waves over soft muds: A two layer fluid model. *J. Phys. Oceanogr.* 8:1121–1131
11. Damodaran R (1973) Studies on the benthos of the mudbank regions of Kerala Coast. Bulletin of the Department of Marine Sciences, University of Cochin. 6:1-126
12. De Wit, PJ (1995) Liquefaction of cohesive sediment by waves. Ph.D. dissertation, Delft Univ. of Technology, Netherlands
13. Dee DP, Uppala S, Simmons AJ, Berrisford P, Poli P, Kobayashi S, Andrae U, Balmaseda MA, Balsamo G, Bauer P, Bechtold P, Beljaars ACM, Berg L, Bidlot J, Bormann N, Delsol C, Dragani R, Fuentes M, Geer AJ, Haimberger L, Healy SB, Hersbach H, Hólm EV, Isaksen L, Kållberg P, Köhler M, Matricardi M, McNally AP, Monge-Sanz BM, Morcrette JJ, Park BK, Peubey C, Rosnay P, Tavolato C, Thépaut JN, Vitart F (2011) The ERA-Interim reanalysis: configuration and performance of the data assimilation system. *Quarterly Journal of the Royal Meteorological Society* 137(656):553-597
14. Elgar S, Raubenheimer B (2008) Wave dissipation by muddy seafloors. *Geophys. Res. Lett.* 35, 5pp.
15. Faas, RW (1991), Rheological boundaries of mud: where are the limits?, *Geo-Marine Letters* 11, 143–146.
16. Faas RW (1995) Rheological characteristics of Allepey mud and their role in the formation and maintenance of mudbanks on the Kerala coast of south west of India. *Journal of Coastal Research.* 11:188–193
17. Froidefond J.M., Pujos M., and Andre X.(1988), Migration of mud-banks and changing coastline in French Guiana, *Marine Geology*, 84, pp.19-30.
18. Gade HG (1958) Effects of a non-rigid, impermeable bottom on plane surface waves in shallow water. *J. Mar. Res.* 16:61–82
19. Gopinathan CK, Qasim S (1974) Mudbanks of Kerala - their formation and characteristics. *Sciences* 3:105-114
20. Hasselmann S, Hasselmann K (1985) Computations and parameterizations of the nonlinear energy transfer in a gravity-wave spectrum, Part I: A new method for efficient computations of the exact nonlinear transfer integral. *J. Phys. Oceanogr.* 15:1369–1377
21. Hsiao SV, Shemdin OH (1980) Interaction of ocean waves with a soft bottom. *J. Phys. Oceanogr.* 10:605–610
22. Hsu TJ, Ozdemir CE, Traykovski PA (2009) High-resolution numerical modeling of wave-supported gravity-driven mud flows. *J. Geophys. Res.* 114, C05014, doi:10.1029/2008JC005006
23. Hsu WY, Hwung HH, Hsu TJ, Torres-Freyermuth A, Yang R (2013) An experimental and numerical investigation on wave-mud interactions. *J. Geophys. Res.* 118, doi:10.1002/jgrc.2013
24. Jacob, N., Ansari, M. A., Revichandran, C. (2015), Environmental isotopes to test hypotheses for fluid mud (mud bank) generation mechanisms along the southwest coast of India, *Estuarine, Coastal and Shelf Science*, 164:115-123.
25. Jamali, M, Seymour B, and Lawrence G (2003), Asymptotic analysis of a surface-interfacial wave interaction, *Phys. Fluids*, 15, 47–55.
26. Jaramillo S, Sheremet A, Allison MA, Reed AH, Holland KT (2009) Wave-mud interactions over the muddy Atchafalaya subaqueous clinoform, Louisiana, United States: Wave-supported sediment transport. *J. Geophys. Res.* 114, C04002, doi:10.1029/2008JC004821
27. Jiang F, Mehta AJ (1995) Mudbanks of the southwest coast of India .4. Mud viscoelastic properties. *Journal of coastal research.* 11(3):918-926

28. Jiang F, Mehta AJ (1996) Mudbanks of the southwest coast of India .5. Wave attenuation. *Journal of coastal research* 12(4):890-897
29. Kaihatu JM, Sheremet A, Holland KT (2007) A model for the propagation of nonlinear surface waves over viscous muds. *Coastal Eng* 54(10):752-764
30. Kranenburg W, Winterwerp J, Boer G de, Cornelisse J, Zijlema M (2011) SWAN-Mud: Engineering model for mud-induced wave damping. *J. Hydraul. Eng.* 137(9):959-975
31. Kurup PG (1977) Studies on the physical aspects of the mudbanks along the Kerala coast with special reference to the Purakkad mud bank. Ph.D. Thesis, University of Cochin
32. Loveson, V J, Dubey, R, Dinesh Kumar, Nigam, R, Naqvi, SWA (2016), An insight into subterranean flow proposition around Alappuzha mudbank coastal sector, Kerala, India: inferences from the subsurface profiles of Ground Penetrating Radar, *Environ Earth Sci*,75:1361, DOI 10.1007/s12665-016-6172-6.
33. Maa PY (1986) Erosion of soft muds by waves. Ph.D. Dissertation, University of Florida, Gainesville, Florida
34. MacPherson H, Kurup PG (1981) Wave damping at the Kerala mudbanks. *Indian J. Mar. Sci.* 10:154-160
35. Mallik TK, Mukherji KK, Ramachandran KK (1988) Sedimentology of the Kerala mudbanks (Fluid muds?). *Mar. Geol.* 80:99-118
36. Mathew J (1992) Wave-mud interaction in mudbanks, PhD Thesis, Cochin: Cochin University of Science and Technology, 132p.
37. Mathew J, Baba M, Kurien NP (1995) Mudbanks of SW coast of India I: wave characteristics. *Journal of Coastal Research* 11:168–178
38. Mathew J, Baba M (1995) Mudbanks of SW coast of India II: wave-mud interaction. *Journal of Coastal Research* 11:178–187
39. Mehta, AJ and Jiang F (1993), Some observations on water wave attenuation over nearshore underwater mudbanks and mudberms. Technical Report of Coastal and Oceanographical Engineering Department, UFL/COEL/MP-93/01, University of Florida, Gainesville, Florida. 45. p.
40. Mei CC, Liu KF (1987) A Bingham-plastic model for a muddy sea bed under long waves. *J. Geophys. Res.* 92:14581–14594
41. Menon, KPP (1924), In: Menon, K.P.P. (Ed.). *A History of Kerala*, vol. 1. Cochin Govt. Press, 562 pp.
42. Nair, RR (1976), Unique mudbanks of Kerala, southwest coast of India. *Bull.Am. Assoc. Pet. Geol.*, 60, 616-621.
43. Nair PVR, Gopinathan CP, Balachandran VK, Mathew KJ, Regunathan A, Rao DS, Murthy AVS (1984) Ecology of mud banks Phytoplankton productivity in Alappuzha mudbank. *Central Marine Fisheries Research Institute Bulletin.* 31:28-34
44. Narayana AC, Jago CF, Manojkumar P, Tatavarti R (2008) Nearshore sediment characteristics and formation of mudbanks along the Kerala coast, southwest India. *Estuarine, Coastal and Shelf Science.* 78:341-352
45. Ng CN (2000) Water waves over a muddy bed: A two-layer Stokes boundary layer model. *Coastal Eng.* 40:221–242
46. Philip, AS, Babu, CA, Hareeshkumar, PV (2013), Meteorological aspects of mud bank formation along south west coast of India, *Continental Shelf Research* 65:45–51.
47. Ramachandran KK (1989) Geochemical characteristics of mudbank environment - a case study from Quilandy, west coast of India. *J. Geol. Soc. India* 33:55-63
48. Rao DS, Regunathan A, Mathew KJ, Gopinathan CP, Murthy AVS (1984) Mud of the mudbank : Its distribution and physical and chemical characteristics. *Central Marine Fisheries Research Institute Bulletin.* 31:21-25

49. Reddy, MPM and Varadachari, VVR (1973), Sediment movement in relation to wave refraction along west coast of India. *Proc. Indian Geophys. Union.*, 10: 169-182.
50. Ren ME, Shi YL (1986) Sediment discharge of the Yellow River (China) and its effect on the sedimentation of the Bohai and the Yellow Sea. *Continental Shelf Research*, 6 (6), pp 785–810.
51. Rogers WE, Holland KT (2009) A study of dissipation of wind-waves by mud at Cassino Beach, Brazil: Prediction and inversion. *Continental Shelf Research* 29 (3):676–690
52. Rogers WE, Orzech MD (2013) Implementation and Testing of Ice and Mud Source Functions in WAVEWATCH III, NRL Memorandum Report, NRL/MR/7320--13-9462
53. Safak I, Sheremet A, Allison MA, Hsu TJ (2010) Bottom turbulence on the muddy Atchafalaya Shelf, Louisiana, USA. *J. Geophys. Res.* 115, C12019, doi:10.1029/2010JC006157
54. Safak I, Sahin C, Kaihatu JM, Sheremet A (2013) Modeling wave-mud interaction on the central chenier-plain coast, western Louisiana shelf, USA. *Ocean. Modelling.* 70:75-84
55. Samiksha SV, Vethamony P, Aboobacker VM, Rashmi R (2012) Propagation of Atlantic Ocean swells in the north Indian Ocean: a case study. *Nat. Haz. Ear. Sys. Sci.* 12:3605-3615
56. Shenoi SSC, Murty CS (1986) Viscous damping of solitary waves in the mudbanks of Kerala. *Indian J. Mar. Sci.* 15:78-83
57. Sheremet A, Jaramillo S, Hsu SF, Allison MA, Holland KT (2011) Wave-mud interactions over the muddy Atchafalaya subaqueous clinoform, Louisiana, United States: Wave processes, *J. Geophys. Res.* 116, C06005, doi: 10.1029/2010JC006644. <http://dx.doi.org/10.1029/2010JC006644>
58. Sheremet A, Mehta AJ, Liu B, Stone GW (2005) Wave-sediment interaction on a muddy inner shelf during Hurricane Claudette. *Estuarine Coastal Shelf Sci.* 63:225–233
59. Shynu, R, Rao, VP, Samiksha, SV, Vethamony, P, Naqvi, SWA, Kessarkar, PM, Babu, MT, Dineshkumar, PK, (2017), Suspended matter and fluid mud off Alappuzha, southwest coast of India, *Estuarine, Coastal and Shelf Science*, vol.185(5); 2017; 31-43.
60. Siadatmousavi SM, Allahdadi M, Chen Q, Jose F, Roberts HH (2012) Simulation of wave damping during a Cold Front over the Muddy Atchafalaya Shelf. *Continental Shelf Research* 47:165–177
61. Silas EG (1984) Coastal zone management: Mudbanks of Kerala coast. *Central Marine Fisheries Research Institute Bulletin.* 31:1-74
62. Tatavarti Rao, Narayana, AC (2006) Hydrodynamics in a Mudbank regime during Non-Monsoon and Monsoon Seasons. *Journal of Coastal Research* 22(6):1463-1473
63. The SWAN team, User manual, SWAN Cycle III, version 41.01A, Delft University of Technology, 2015
64. Thompson MPK (1986) Seasonal distribution of cyclopoid copepods of the mud banks off Alappuzha, Kerala coast. *Journal of the Marine Biological Association of India* 28 (1&2) 48-56
65. Tolman HL (1991) A third-generation model for wind-waves on slowly varying, unsteady, and inhomogeneous depths and currents. *Journal of Physical Oceanography* 21:782–797
66. Tolman HL (2002) Alleviating the garden sprinkler effect in wind wave models. *Ocean Mod.* 4:269–289

67. Tolman HL, the WAVEWATCH III<sup>®</sup> Development Group (2014) User Manual and System Documentation of WAVEWATCH III<sup>®</sup> version 4.18, Tech. Note 316, NOAA/NWS/NCEP/MMAB, 282 pp. + Appendices
68. Traykovski P, Geyer WR, Irish JD, Lynch JF (2000) The role of wave-induced fluid mud flows for cross-shelf transport on the Eel River continental shelf. *Cont. Shelf Res.* 20:2113–2140
69. Traykovski P, Wiberg P, Geyer WR (2007) Observations and modeling of wave-supported sediment gravity flows on the Po pro delta and comparison to prior observations from the Eel shelf. *Cont. Shelf Res.* 27:375–399. doi:10.1016/j.csr.2005.07.008.
70. Vinzon SB, Mehta AJ (1998) Mechanism for formation of luctocline by waves, *J. Waterw. Port Coastal Ocean Eng.* 124(3):147–149
71. Wells, JT and Coleman, JM (1981), Physical processes and finegrained sediment dynamics, coast of Surinam, South America. *J. Sediment. Petrol.*, 51, 1053 – 1068.
72. Wells, JT and Kemp, GP (1986), Interaction of surface waves and cohesive sediments: Field observations and geologic significance. In: *Esturine cohesive sediment dynamics* (Ed. A.J. Mehta), Springer-Verlag, Berlin, 43-65.
73. Winterwerp JC, Graaff RFD, Groeneweg J, Luijendijk AP (2007) Modeling of wave damping at Guyana mud coast. *Coastal Eng.* 54:249–261
74. Yamamoto T, Takahashi S (1985) Wave damping by soil motion, *J. Waterway Port Coastal Ocean Eng.* 3: 62–77
75. Zhang X, Ng CO (2006) Mud–wave interaction: a viscoelastic model. *China Ocean Engng* 20:15–26



## List of Tables

**Table 1.** Statistical comparison of WW3 model  $H_s$  for no-mud condition with ERA-Interim and measured  $H_s$  at 15m water depth (B1).

**Table 2.** Statistical comparison of measured  $H_s$  with model  $H_s$  for varying mud thickness, viscosity and density for DL and Ng methods (21 May - 31 July 2014).

## List of Figures

**Figure 1.** (a) The outer domain covering the Indian Ocean; (b) Inner domain with bathymetry details and wave rider buoy moored locations, B1 and B2; (c) The box covers all the 12 mudbanks regions (not to scale) off Kerala; (d) Mud patch introduced in the model.

**Figure 2.** Wave parameters measured at 15m (B1) and 7m (B2) water depths; also shown is wind speed and direction (bottom panel) measured using an AWS at a nearby coastal station.

**Figure 3.** Measured  $H_s$  plot is divided into time segments as I, IIa, IIb, IIIc, IIId and IIIe in order to explain the dynamics of MB at the measurement locations and subsequent wave energy dissipation.

**Figure 4.** Variation of  $H_s$  and  $T_p$  measured at 15m (B1) and 7m (B2) water depths during wave energy dissipation in the MB region. This part of the figure is expanded from Part II (a&b) and Part III (c,d&e) of Figure 5 to illustrate the wave spectral behaviour at B1 and B2.

**Figure 5.** Typical measured wave spectra during the MB period: (a) 01-07-2014, (b) 05-07-2014, (c) 11-07-2014, (d) 14-07-2014, (e) 19-07-2014 and (f) 25-07-2014 at B1 and B2.

Figure 6. Evolution of wave frequency spectrum during mudbanks formation at the two water depths off Alappuzha: (a) 15 m (location B1) and (b) 7m (location B2).

**Figure 7.** Energy fluxes (represented in colour; units  $Wm^{-1}$ ) based on observations at (a) 15 m depth, (b) 7 m depth and (c) difference between the fluxes at 15m and 7m.

**Figure 8.** Comparison of (a) measured  $H_s$  at B1 (depth=15m) with  $H_s$  of ERA-I and  $H_s$  of WW3 (no-mud condition), (b) measured  $H_s$  at B1 with  $H_s$  of WW3 model (mud condition: DL and Ng), (c) measured  $T_m$  at B1 with  $T_m$  of WW3 (no-mud condition and mud condition) and (d) measured  $D_p$  with  $D_m$  of WW3 (no-mud condition and mud condition).

**Figure 9.** Comparison of measured  $H_s$  with modelled  $H_s$  for varying mud viscosity, thickness and density for DL (a, b & c) and Ng (d & e) methods at location B1. Legend numbers correspond to the test cases shown in Table 2.